The Mechanism of Pore Assembly for a Cholesterol-Dependent Cytolysin: Formation of a Large Prepore Complex Precedes the Insertion of the Transmembrane β-Hairpins†

Laura A. Shepard,‡ Oleg Shatursky,‡ Arthur E. Johnson,§ and Rodney K. Tweten*,‡

Department of Microbiology and Immunology, University of Oklahoma Health Sciences Center, BMSB, Room 1053, 940 Stanton L. Young Boulevard, Oklahoma City, Oklahoma 73190, and Departments of Medical Biochemistry and Genetics, of Chemistry, and of Biochemistry and Biophysics, Texas A&M University, College Station, Texas 77843

Received February 25, 2000; Revised Manuscript Received June 1, 2000

ABSTRACT: Perfringolysin O (PFO) is a member of the cholesterol-dependent cytolysin (CDC) family of membrane-penetrating toxins. The CDCs form large homooligomers (estimated to be comprised of up to 50 CDC monomers) that are responsible for generating a large pore in cholesterol-containing membranes of eukaryotic cells. The assembly of the PFO cytolytic complex was examined to determine whether it forms an oligomeric prepore complex on the membrane prior to the insertion of its membrane-spanning β-sheet. A PFO oligomeric complex was formed on liposomes at both 4 °C and 37 °C and shown by SDS−agarose gel electrophoresis to be comprised of a large, comparatively homogeneous complex instead of a distribution of oligomer sizes. At low temperature, the processes of oligomerization and membrane insertion could be resolved, and PFO was found to form an oligomer without significant membrane insertion of its β-hairpins. Furthermore, PFO was found to increase the ion conductivity through a planar bilayer by large and discrete stepwise changes in conductance that are consistent with the insertion of a preassembled pore complex into the bilayer. The combined results of these analyses strongly support the hypothesis that PFO forms a large oligomeric prepore complex on the membrane surface prior to the insertion of its transmembrane β-sheet.

Perfringolysin O (PFO),[1] a pore-forming toxin which is produced and secreted by the Gram-positive anaerobe *Clostridium perfringens*, is a member of the large family of cholesterol-dependent cytolysins (CDCs) [previously referred to as the thiol-activated cytolysins; reviewed in (*1*−*3*)]. These cytolytic toxins are produced by at least five genera of bacterial pathogens. For the better part of the last 3 decades, the membrane structure of the CDCs has been extrapolated from electron micrographs of complexes of these toxins imaged on various natural and synthetic membranes (*4*−*7*). These analyses revealed that the CDCs formed large oligomeric complexes on the membrane, and it was subsequently shown that these large complexes were comprised of polymers of the monomeric toxin (*7*). However, analysis of these membrane complexes by electron microscopy (EM) did not provide information on the processes that led to the formation of these large membrane-embedded complexes from the soluble, monomeric toxins. Until recently, little structural information was available on both the soluble and membrane-bound forms of the CDCs.

We recently solved the crystal structure of the soluble monomeric form of PFO (*8*), and subsequently identified two membrane-spanning β-hairpins (*9, 10*) that are located within domain 3 of the soluble monomer. Therefore, the primary function of domain 3 is to form the membrane-spanning β-hairpins, although it is possible that it is also involved in intermolecular subunit interactions during oligomer formation. Penetration of the membrane by PFO was shown to require the conversion of six short α-helices in domain 3 into two membrane-spanning β-hairpins. Since the six α-helices comprise 11% of the primary structure of PFO, membrane insertion involves a major change in the secondary and tertiary structure of domain 3. However, the precise sequence of events in the formation of the large PFO pore remains unclear: Does oligomerization of PFO precede the insertion of its transmembrane domains or does insertion precede oligomerization or occur concomitantly with oligomer formation?

It has been shown in recent years that pore-forming toxins such as aerolysin, *Clostridium septicum* α-toxin, and *Staphylococcus aureus* α-hemolysin, as well as the protective antigen of anthrax toxin, form oligomeric prepore complexes

† These studies were supported by a grant to R.K.T. from the National Institutes of Health (AI37657), by the Robert A. Welch Foundation (A.E.J.), and by a National Science Foundation fellowship (GRE0355771) to L.A.S.

* Correspondence should be addressed to this author at the Department of Microbiology and Immunology, 940 Stanton L. Young Blvd., The University of Oklahoma Health Sciences Center, Oklahoma City, OK 73190. Phone: (405) 271-2133. Fax: (405) 271-3117. E-mail: Rod-Tweten@ouhsc.edu.

‡ University of Oklahoma Health Sciences Center.

§ Texas A&M University.

[1] Abbreviations: PFO, perfringolysin O; nS, nanoSiemens; TMH, transmembrane β-hairpin; POPC, 1-palmitoyl-2-oleoyl-*sn*-glycero-3-phosphocholine; IANBD, *N*,*N*′-dimethyl-*N*-(iodoacetyl)-*N*′-(7-nitrobenz-2-oxa-1,3-diazolyl)ethylenediamine; HBS buffer, HEPES-buffered saline.

10.1021/bi000436r CCC: $19.00
Published on Web 07/27/2000

prior to the insertion of their channel-forming β-barrel (*11*−*14*). The formation of the prepore complex presumably allows the toxin monomers to come together and form the precursor structure of the β-barrel, thereby permitting these polypeptide stretches to insert into the membrane in a single, concerted action to form the transmembrane β-barrel. The membrane-spanning β-barrel formed by α-hemolysin and anthrax protective antigen is comprised of seven β-hairpins (*15, 16*). Based on these examples, Rossjohn et al. (*8*) proposed that the formation of an oligomeric prepore complex precedes its membrane insertion. However, the number of monomers that comprise the CDC oligomer has been estimated at 24−50 monomers (*6, 17*), and each monomer contributes 2 hairpins to the membrane-spanning β-barrel (*10*). Based on these estimates, the CDCs could form a membrane-spanning β-sheet containing as many as 100 β-hairpins. The large size of the resulting CDC membrane-spanning β-sheet therefore raises a critical issue: Can the insertion of so many β-hairpins be coupled so that they are all inserted at the same time?

Palmer et al. (*18*) recently proposed a novel assembly model for streptolysin O (SLO), a CDC that shares about 65% identity with the primary structure of PFO. Because of the large size of the CDC oligomer and the perceived heterogeneity of the oligomer, it was suggested that a prepore-based mechanism could not explain the membrane insertion of the CDCs. Instead, they suggested that a small oligomeric complex of SLO, possibly as small as a dimer, initially inserts into the membrane to form a small pore. This small oligomer and its pore would then be enlarged in a progressive fashion by the addition of individual soluble toxin monomers. Each monomer is predicted to simultaneously insert its transmembrane domain and bind to the growing end of the oligomer. This model of oligomer assembly is a fundamental shift in the current perception of how cytolytic toxins form a homooligomer and insert their transmembrane domains. However, to date, no toxin has been shown unambiguously to assemble a transmembrane oligomer using this type of mechanism. This model is also inconsistent with the earlier findings of Harris et al. (*19*) in which we determined that the oligomerization of PFO preceded the onset of erythrocyte hemolysis. The data of Harris et al. also suggested that a prepore complex was forming prior to the onset of hemolysis, although at the time of their experiments this concept had not been proposed for bacterial pore-forming toxins.

To gain a better understanding of the assembly and membrane insertion of the CDCs, we examined this process using PFO, the only member of this family for which both the crystal structure of the soluble monomer has been solved (*8*) and the residues involved in transmembrane β-hairpin formation have been identified (*9, 10*). Two key features separate the prepore model from the continuous growth model. First, oligomerization of the toxin into a prepore complex occurs in the absence of significant membrane insertion, whereas membrane insertion either precedes or is coupled to oligomerization in the continuous growth model. Second, the prepore model predicts that the oligomer would achieve a specific size prior to insertion, whereas the continuous growth model predicts that the oligomers and pores would be heterogeneous with a wide distribution of sizes. In the current study, we have utilized a combination of analyses including fluorescence spectroscopy, electron microscopy, planar bilayers, and SDS−agarose gel electrophoresis (SDS−AGE) to examine the temporal sequence of oligomer formation and the insertion of the membrane-spanning β-sheet of PFO. The results of these studies strongly support a cytolytic mechanism that requires the formation of a large oligomeric prepore complex on the membrane surface as a precursor to membrane penetration and pore formation.

MATERIALS AND METHODS

Bacterial Strains, Plasmids, and Chemicals. The recombinant mutant PFO^{C459A}, and cysteine-substituted derivatives thereof, were used for all studies herein. The construction and characteristics of these mutants have been previously described in detail (*9*). PFO^{C459A} is a fully active, cysteine-less derivative of wild-type PFO in which C459 was converted to an alanine residue. All phospholipids and sterols were obtained from Avanti Polar Lipids (Alabaster, AL), and all chemicals and enzymes were obtained from Sigma Chemical Co. (St. Louis, MO) unless otherwise specified.

Modification of Cysteine-Substituted PFO with the Fluorescent Dye NBD. Cysteine-substituted derivatives of PFO^{C459A} were derivatized as previously described (*9*) via the sulfhydryl group of cysteine with *N*,*N*′-dimethyl-*N*-(iodoacetyl)-*N*′-(7-nitrobenz-2-oxa-1,3-diazolyl)ethylenediamine (IANBD) (Molecular Probes, Eugene, OR). Prior to labeling, the toxin was passed over a column (1.6 × 25 cm) containing Sephadex G-75 fine to remove excess dithiothreitol (DTT) and transfer the toxin into the appropriate buffer for labeling [50 mM HEPES (pH 8.0), 100 mM NaCl]. The modification reaction was carried out using a 10-fold molar excess of dye to toxin in the presence of 3 M guanidine hydrochloride at room temperature (22 °C) for 2 h. The labeling reaction was quenched by the addition of 5 mM DTT, and then passed over a column containing Sephadex G-50 to remove the free dye and the guanidine hydrochloride. The protein-containing fractions were pooled, made 10% (v/v) in glycerol, aliquoted, and stored at −80 °C until used.

Preparation of Liposomes. 1-Palmitoyl-2-oleoyl-*sn*-glycero-3-phosphocholine (POPC) and cholesterol, at a ratio of 45:55 mol % in chloroform, were dried down under a stream of argon at 40 °C, resuspended in 3 mL of ether, and dried again under argon at 40 °C and then dried under vacuum for an additional 3 h. The dried lipid/sterol mixture was resuspended in 3 mL of HBS buffer [50 mM HEPES (pH 7.5), 100 mM NaCl] and vortexed vigorously until a completely uniform suspension was obtained. The lipid mixture was carried through 3 freeze−thaw cycles using liquid nitrogen and room temperature (22 °C) water. The lipid mixture was then passed 21 times through an Avestin Liposofast extruder, using a polycarbonate membrane with a 100 nm pore size to generate unilamellar liposomes (*20*). The liposomes were stored under argon at 4 °C and used within 7 days of preparation.

Gel Electrophoresis and Immunoblot Analyses. Denaturing agarose gel electrophoresis (SDS−AGE) was carried out as follows. SeaPlaque agarose (FMC, Rockland, ME) was mixed with sodium dodecyl sulfate (SDS) gel reservoir buffer (*21*) at a final concentration of 1% (w/v) and heated to 100 °C to melt the agarose. The molten agarose (150 mL) was allowed to cool to 45 °C and then was poured into a chilled

and leveled 20 cm × 20 cm horizontal gel casting tray (Bio-Rad, Hercules, CA) with or without GelBond (Pharmacia, Piscataway, NJ) on the bottom of the tray. If the gel was to be stained, it was poured with GelBond as a support, whereas if it was to be transferred to nitrocellulose paper (MSI, Westborough, MA) for detection of the PFO with antibody, the gel was poured without the GelBond support. The gel was placed into a BioRad SubCell GT horizontal gel electrophoresis system and immersed in SDS reservoir buffer (*21*). Samples were prepared by the addition of a one-fifth volume of sample buffer [0.1% (w/v) bromphenol blue, 40% (v/v) glycerol, and 25% SDS (w/v) made up in reservoir buffer]. The samples were maintained at room temperature until loaded onto the gel. In addition to preparing the sample for SDS−AGE, the addition of the sample buffer was found to immediately stop the oligomerization of PFO in samples incubated with liposomes. For most experiments, these samples were separated by SDS−AGE without heating the sample to 95 °C, unless noted otherwise. Samples were loaded into the wells, and the gel was run at 100 V for approximately 3 h.

For staining with Coomassie Brilliant Blue R, the gel was rinsed overnight in 300 mL of a fixative solution comprised of 10% (v/v) acetic acid and 30% (v/v) methanol in distilled water. The gel (poured on GelBond) was then removed from the fixative solution and air-dried in a Hoefer (San Francisco, CA) Easy Breeze gel dryer. Staining of the dried gel was accomplished with 0.2% (w/v) Coomassie Brilliant Blue R dissolved in the fixative solution. The dried gel was then destained with the fixative solution.

For detection with affinity-purified antibody specific for PFO, the proteins separated by SDS−AGE were transferred to nitrocellulose in a Genie Electrophoretic blotter (Idea Scientific, Minneapolis, MN) according to the manufacturer's instructions. For colorimetric detection of PFO, the blot was prepared and developed as described previously for blots from acrylamide gels (*22*), except that affinity-purified rabbit IgG to PFO was used as the primary antibody. For chemiluminescent detection of low concentrations of PFO and its oligomer, the ECL-Plus kit was used for detection of the anti-PFO as described by the manufacturer (Amersham, Arlington Heights, IL). Protein bands recognized by the antibody were visualized by exposing the immunoblot to Kodak X-Omat AR X-ray film (Kodak, Rochester, NY).

Membrane Insertion and Oligomerization Kinetics. Membrane insertion of the membrane-spanning domain of PFO was monitored by the change in fluorescence intensity of the fluorescent dye NBD that is attached to PFO^{A215C} and is buried in the bilayer when TMH1 inserts into the bilayer (*9, 10*). When covalently attached to C215 via the sulfhydryl group, the fluorescence intensity of NBD increases approximately 7-fold as C215 enters the membrane. Thus, the increase in the fluorescence intensity of the NBD was used to monitor membrane insertion of PFO in these experiments. All fluorescence measurements were performed on an SLM-8100 spectrofluorometer (SLM Instruments) as described previously for transmembrane domain insertion studies (*9*). The excitation wavelength was set to 478 nm, and the emission wavelength was set to 530 nm.

For kinetic analysis of membrane insertion and oligomerization, excess liposomes (previously determined by titration with NBD-labeled PFO^{A215C}) were combined with 136 μg (2.4 nmol) of NBD-labeled PFO^{A215C} in a total volume of 788 μL and maintained at 4 °C. All components were maintained on ice until mixed in a tube that was previously equilibrated at 4 °C in a refrigerated water bath. Two 46 μL samples were removed from this mixture at 0, 5, 15, 30, 45, 60, and 90 min after mixing the toxin and liposomes. One of the samples was placed immediately into a microfuge tube containing 5 μL of SDS sample buffer and 5 μL of 25% (w/v) SDS to stop oligomerization and prepare the sample for SDS−AGE. The second sample was placed into a 3 mL fluorometer cuvette that contained 2 mL of HBS buffer that had been equilibrated to 4 °C in the fluorometer. The fluorescence intensity of this sample was recorded using a 10 s integration time. The extent of the insertion of PFO into the bilayer was then determined by recording the change in NBD intensity that occurred as the dye attached to C215 inserted into the membrane (*9, 10*). In all cases, the fluorescence intensity of the NBD-labeled PFO^{A215C} in the absence of liposomes was used as the negative control for insertion, and its intensity reading was subtracted from the experimental intensity readings. To determine maximum insertion of the dye at the end of the 90 min incubation, the sample was placed into a 37 °C water bath for 20 min to allow PFO to completely oligomerize and insert TMH1 into the liposome membrane. After the incubation at 37 °C, two more 46 μL aliquots were removed and treated as above. It should be noted that after incubation at 37 °C the fluorescence of the sample used to determine the maximum insertion of TMH1 was determined at 4 °C to minimize any temperature effect on the fluorescence intensity. The extent of TMH1 insertion was then calculated by the ratio of the fluorescence intensity of the NBD determined for the various samples taken over time at 4 °C to the fluorescence intensity of the sample that had been incubated at 37 °C. The extent of oligomer formation was determined by densitometry of the Coomassie-stained bands representing the monomeric and oligomeric PFO.

The same procedures were used to determined the extent of insertion of residues S194 and N197, also in TMH1, and K299 and I303 in TMH2. In those experiments where PFO was labeled with NBD, the apparent size of the complex was unaffected.

Electron Microscopy of PFO. Samples were fixed onto Formvar−carbon grids for 1 min and then negatively stained with a 2% (w/v) solution of neutralized phosphotungstic acid for 30 s. Samples were examined and photographed on a JEOL 2000 FX transmission electron microscope (JEOL Ltd., Tokyo, Japan) operated at 200 kV.

To visualize the oligomer present in the protein band seen on the SDS−agarose gels, a sample of PFO^{C459A}, spiked with fluorescein-labeled PFO^{A215C}, was allowed to incubate with liposomes at 37 °C for 30 min. The proteins were then resolved by SDS−AGE as described above. The oligomer band was identified by the fluorescence of the fluorescein-tagged PFO and excised from the gel. The oligomeric protein was extracted from the agarose using BioRad Quantum Prep Freeze N′ Squeeze DNA gel extraction spin columns (Bio-Rad, Hercules, CA) and prepared as described above for EM.

Planar Bilayer Membrane Measurements. Planar membranes were made from fresh heptane solutions of POPC and cholesterol mixed at a ratio of 45:55 mol %, respectively.

Membranes were formed across a 180 μm diameter hole in a Delrin cup of a Warner bilayer chamber (Warner Instruments Corp., Hamden, CT). Total lipid concentration in the heptane solution was 20 mg/mL. The solution bathing the membrane contained 100 mM NaCl and 10 mM Tris-HCl (pH 7.4). The membrane capacitance of the bilayer was monitored until it stabilized. Stable bilayer capacitance was 100−120 pF with the membrane separating equal bath volumes (1 mL) between the Delrin cup and the outer polystyrene chamber (Warner Instruments Corp.). Both chambers could be stirred as required. The cis-compartment was clamped, and the transmembrane current recordings were made using silver chloride electrodes immersed in a 0.2 M KCl solution with 0.2 M KCl agar bridges. The trans-electrode was connected to the Warner high-resolution amplifier headstage and placed inside of the Delrin cup. The potential difference was referenced to the trans-side of the membrane that was defined as zero. The polarization potential between the electrodes did not exceed 1−1.5 mV. The voltage was applied and controlled via a Warner amplifier with 1 kHz bandwidth. Membrane currents were recorded on an XY-recorder or a digital tape drive (A. R. Vetter Co., Rebersburg, PA).

RESULTS

Identification of the Oligomeric Complexes of PFO by Gel Electrophoresis. To date, the CDC oligomer has not been identified by a gel-based electrophoretic method, primarily due to the large size of these complexes. Since the size of the CDC oligomer is estimated, based on electron microscopy, to be in the range of 24−50 monomers (approximately 1.5−2.5 MDa), the size of the complex would preclude it from entering a denaturing polyacrylamide gel. We therefore used an agarose-based SDS gel system to directly examine the distribution of the oligomers formed under various conditions. Denaturing agarose gel systems are capable of separating large complexes up to 5 MDa in mass, depending upon the concentration of the agarose, and have been used extensively for the separation of large polymers such as fibrin and von Willebrand factor (*23, 24*).

The PFO (PFO^{C459A}) oligomer that was formed on liposomes at 37 °C was treated with glutaraldehyde prior to treatment with SDS and heat in order to prevent the dissociation of the oligomer. Early studies of the CDC oligomer suggested that the PFO oligomer might have been dissociated by SDS (*25*). After separating the complexes by SDS−AGE, we observed a remarkably homogeneous oligomer band on the agarose gel (Figure 1A, lane 3). A low level of oligomers larger than the predominant oligomer band size was also observed.

An aliquot of the same sample of PFO^{C459A} was prepared as described above, but the cross-linking step was omitted (Figure 1, lane 4). In the absence of cross-linker, about 50% of the oligomeric complex was dissociated to monomer, but the remaining PFO was in the form of a homogeneous higher mass oligomer. The apparent increase in mass of the remaining oligomer probably results from the relaxation of the oligomeric complex (i.e., the un-cross-linked oligomers likely exhibited a more open or extended structure after heating) in the absence of the cross-linker.

We also examined the stability of the PFO oligomer after it was treated with SDS, but was not heated to 95 °C (Figure 1A, lanes 5 and 6). Under these conditions, the PFO oligomer migrated as a single band on the gel regardless of whether it was cross-linked (Figure 1A, lane 5) or not (Figure 1A, lane 6). Therefore, the PFO oligomer is resistant to dissociation by SDS and partially resistant to dissociation by the combination of SDS and heat. These characteristics are similar to those described for the small, heptameric oligomers of aerolysin (*11*), and *Staphylococcus aureus* α-hemolysin (*26*) and *Clostridium septicum* α-toxin (*22*) which exhibit significant or complete resistance to dissociation by heat and SDS. The resistance of the PFO oligomer to dissociation suggests that the forces that facilitate the interaction of the PFO monomers in the oligomer may be similar to those that stabilize the smaller oligomers of aerolysin, α-hemolysin and α-toxin.

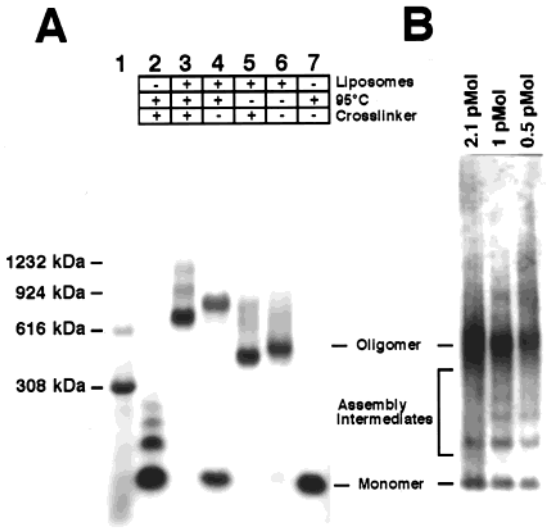

FIGURE 1: SDS−agarose gel analysis of PFO^{C459A} oligomers. The size distribution of the oligomer formed by PFO binding to liposomes at 4 °C was determined by SDS−AGE of liposome-bound PFO. Panel A: Lane 1 contains *Clostridium difficile* toxin A as a high molecular mass marker. In addition to the monomer form (308 kDa), toxin A also formed dimers (616 kDa), trimers (924 kDa), and tetramers (1232 kDa) in solution. The toxin was prepared with SDS-sample buffer but was not heated to 95 °C so as to not disrupt the polymeric forms of toxin A. Lane 2, soluble PFO was cross-linked with 5 mM glutaraldehyde for 30 min at 37 °C, urea was added to 1 M to stop the cross-linking, and then SDS sample buffer was added and the sample was heated to 95 °C for 10 min. The samples shown in lanes 3−7 were treated as shown above the gel. For those samples that had been cross-linked, the glutaraldehyde concentration was 2.5 mM, and the samples were cross-linked for 1 min prior to being quenched with 1 M urea and prepared for SDS−AGE. In all cases where PFO was incubated with liposomes, the liposomes (45 mol % POPC/55 mol % cholesterol) were incubated with PFO for 30 min at 37 °C. Panel B: Up to 256-fold less PFO was incubated at 37 °C for 30 min with the same amount of liposomes and under the same conditions as used for the experiments in panel A. Samples were then solubilized with SDS sample buffer and separated by SDS−AGE and electrophoretically transferred to nitrocellulose. Detection of the PFO was accomplished by immunoblot analysis and a chemiluminescent substrate as described under Materials and Methods. Shown is the autoradiogram from the immunoblot.

Oligomers were also formed with much lower amounts of PFO in order to determine if limiting the toxin concentration would alter the distribution and size of the main oligomer band (Figure 1B). When as little as 0.5 pmol of PFO (256-

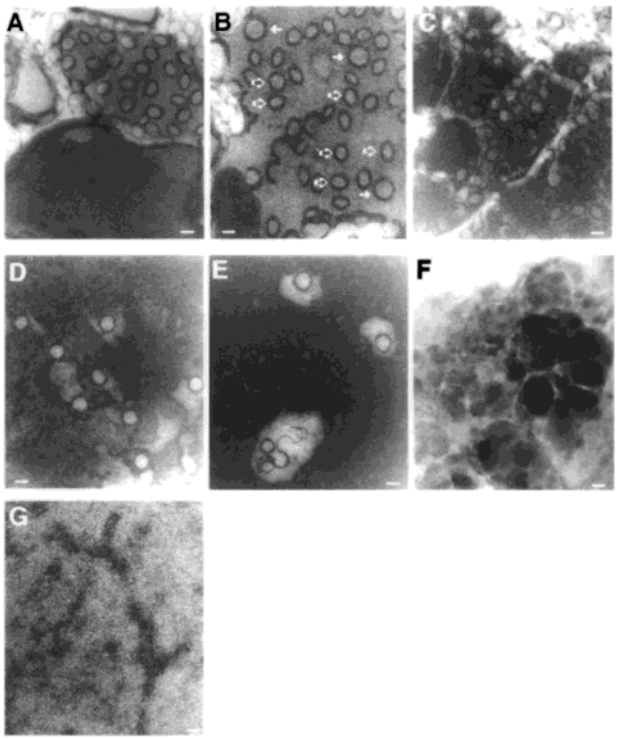

FIGURE 2: Transmission electron micrographs of PFO^{C459A} oligomers. PFO oligomers from samples that were formed under various conditions, solubilized with SDS, or extracted from the predominant oligomer band from an SDS−agarose gel, were imaged by EM to visualize the structure of the PFO oligomers. (A) PFO oligomers formed at 37 °C on liposomes. (B) PFO oligomers as in (A), except that the liposomes were solubilized with SDS before preparation for EM. (C) PFO oligomers present on liposomes at 5 °C. (D) PFO oligomers as in (C), except that the liposomes were first solubilized with SDS. (E) Gel-purified oligomer extracted from the SDS−agarose gel. (F) PFO oligomers as in (B), except that the sample was heated to 95 °C for 10 min. (G) Soluble monomers of PFO. The outlined arrows in panel B show several examples of the most abundant rings, whereas the solid arrows identify examples of the more rare large rings. Magnification is 200000×. Bars = 20 nm.

fold less than the experiments in Figure 1A) was incubated with the same amount of liposomes as used in the experiments shown in Figure 1A, the oligomer band exhibited the same relative migration by SDS−AGE at all concentrations and remained most predominant oligomeric species present. Therefore, PFO exhibits a strong tendency to form a specific size of oligomer over a wide range of concentrations.

Although SDS−AGE is a useful tool to study the distribution of the PFO oligomer, we suggest that any estimations of the molecular mass of the oligomeric complex must be viewed with caution until the mass of the oligomer can be corroborated by another independent method.

Electron Microscopy of the Oligomeric Complexes of PFO. The oligomers detected by SDS−AGE (Figure 1A) were also examined by electron microscopy (EM) to determine if the same ring-shaped structures were present in our oligomer samples that had been treated in various ways. The oligomers that were present on liposome membranes, as well as those present in SDS-solubilized membranes or extracted from the SDS−agarose gels, were examined by EM (Figure 2). EM analysis of the complexes present on liposomes revealed three general forms of PFO oligomer: arcs, elliptical rings, and a few large circular rings (Figure 2A). The ellipsoid-shaped rings were the predominant complexes and exhibited a small degree of heterogeneity in size and shape. Micrographs of PFO oligomers that had been formed at 37 °C on liposomes and then solubilized using SDS, but not heated to 95 °C (Figure 2B), revealed the presence of the same oligomeric structures as observed on the intact liposomes. This observation demonstrates that the structures detected by EM on liposomes are also resistant to dissociation by SDS. Micrographs of oligomers formed at 4 °C exhibited the same structures as observed at 37 °C, both before and after solubilization of the liposomes by SDS (Figure 2C and 2D, respectively), but they were less abundant.

Oligomer purified from the predominant high molecular weight oligomer band present on the SDS−agarose gels also exhibited oligomeric structures similar to those observed on the liposomes (Figure 2E). Ring-shaped structures were the predominant form of oligomer observed in several samples (only one is shown, but all exhibited similar structures), although a few C-shaped structures were also observed. Heating the SDS-treated toxin−liposome mixtures to 95 °C resulted in the loss of detectable structure by EM (Figure 2F), even though an oligomer band with a larger apparent mass was still detected by SDS−AGE (Figure 1A, lane 4). Heating the SDS-treated oligomer eliminated the oligomeric structure observed by EM, probably by destroying the compact structure of the oligomer that was normally visible by EM. EM analysis of soluble PFO monomer in the absence of liposomes revealed no detectable oligomeric structures (Figure 2G).

Oligomer Formation at Various Temperatures. When PFO was incubated at 37 °C with liposomes, significant oligomer formation was apparent after 5 min incubation with the liposomes (Figure 3A). Most of the oligomer is a relatively homogeneous, high molecular weight complex as revealed by SDS−AGE. The majority of the oligomers formed rapidly at 37 °C without significant levels of intermediate-sized complexes (as detected by Coomassie-stained SDS−agarose gels). The same-sized oligomer is also formed at 4 °C, but at a slower rate (Figure 3A). Although the rate of oligomer formation is slower at 4 °C, a significant fraction (55%) of the monomer is converted to oligomer after 60 min, as determined by densitometric analysis of the band intensities on the gel (data not shown). Slowing the rate of oligomer formation by lowering the temperature did not increase the abundance of assembly intermediates (Figure 3A). The lack of detectable intermediates may have resulted from an inherent instability of these intermediates to SDS. However, cross-linking the PFO oligomers had no apparent effect on the low level of assembly intermediates in identical experiments (data not shown), thereby indicating that the absence of detectable intermediates in Coomassie-stained gels was not the result of an inherent instability of the assembly intermediates to treatment with SDS.

Using more sensitive antibody-based methods, low levels of intermediates were detected (Figure 3B) at times as early at 1 min after mixing the PFO monomer and liposomes at 4 °C. However, PFO monomer and the same size predominant oligomer complex observed at 37 °C were still the most abundant species present. The amount of intermediate-sized assembly products reached a low steady-state level that did not increase significantly over 20 min. As found above for the stained gels, cross-linking did not

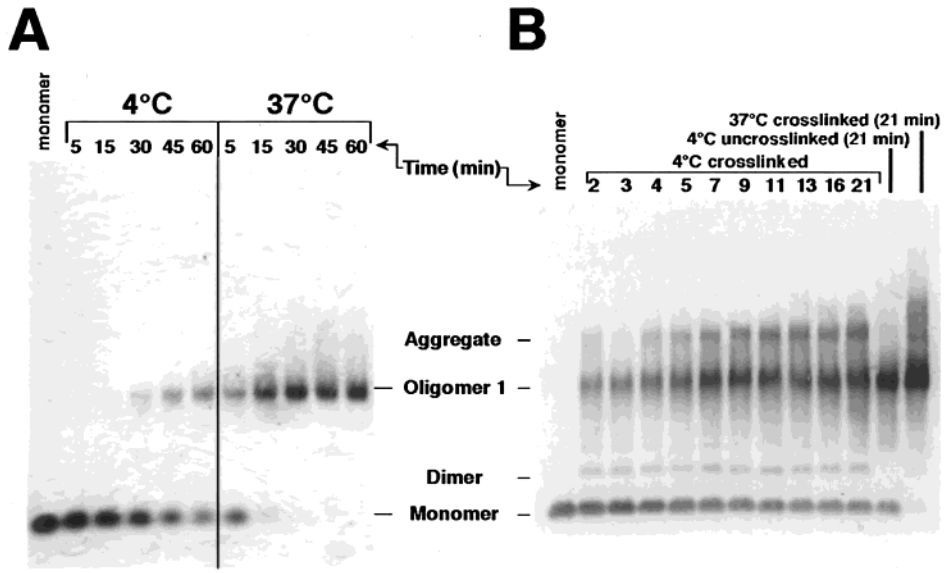

FIGURE 3: Kinetics of oligomer formation at 4 and 37 °C. In panel A, the appearance of the oligomer band is shown in samples of PFO (140 pmol)-treated liposomes which were incubated at 4 or 37 °C. Samples were removed at the times indicated and immediately solubilized in 5% (w/v) SDS without cross-linking and then separated by SDS−AGE (1% w/v). Protein was detected by Coomassie staining of the dried gel. In panel B, the oligomers were detected by immunoblot analysis in samples taken as early as 1 min after mixing the toxin with membranes at 4 °C. The samples were removed and cross-linked for an additional 1 min with 2.5 mM glutaraldehyde to stabilize any intermediates that may have been SDS-sensitive. The times shown on the gels in panel B reflect the time the sample was removed plus the additional minute for cross-linking. A 4 °C un-cross-linked sample and a 37 °C cross-linked sample taken after 20 min of incubation are shown for comparison. Numbers above the lanes indicate the time (in minutes) when the sample was placed into SDS sample buffer to stop the oligomerization process.

appear to change the relative abundance of these intermediates (compare the 21 min samples ± cross-linker), indicating that the intermediates in the assembly of the oligomer remain at low steady-state levels. From these data, it is also evident that, in the earliest stages of oligomer formation observed at low temperature, the predominant oligomeric complex remains the same as that detected after oligomerization has been allowed to go to completion at 37 °C.

An additional higher mass band in the cross-linked samples was also detected at all times during the oligomer assembly when antibody was used to detect the assembly products (Figure 3B, lanes designated 2 min−21 min). However, in the absence of cross-linking, this aggregate was converted to a size that corresponded to the main SDS-resistant oligomer band (Figure 3B, compare the 21 min samples ± cross-linker). When the same experiment shown in Figure 3B was carried out in the absence of cross-linker, the same results were obtained except that the SDS-sensitive higher mass band was significantly decreased (data not shown). Thus, the higher mass band most likely represents the random cross-linking of two of the assembled oligomers.

These data show that the conversion of monomeric PFO to the predominant oligomer occurs rapidly once oligomer formation is initiated, while the assembly intermediates remain at low, steady-state levels.

Oligomer Formation and Membrane Insertion of TMH1 and TMH2. If PFO assembles into a prepore complex, then the formation of the oligomer should precede the insertion of the transmembrane complex. A hallmark of the formation of a prepore oligomer is that oligomer formation occurs prior to a significant insertion of its transmembrane β-sheet (*12*−*14*, *27*). Preliminary studies indicated that the insertion of both transmembrane domains (both TMH1 and TMH2) was significantly reduced at 4 °C (Heuck, Tweten, and Johnson, manuscript in preparation), but as shown in Figure 3 oligomer assembly proceeded at a reasonable rate at this temperature. We reasoned that if the formation of a prepore oligomer precedes the insertion of the transmembrane hairpins, then low temperature might better resolve these two processes. However, if the oligomer formed by the continuous growth model of Palmer et al. (*18*), oligomerization and insertion would have to be tightly linked and should not exhibit significantly different kinetics at any temperature.

When these two processes were measured at 4 °C, a dramatic difference in their rates was observed (Figure 4A). Within 90 min at 4 °C, nearly all of the monomer has been converted to oligomer, whereas the NBD located at position A215, a residue that has been shown previously to face the membrane as part of TMH1(*9*), exhibited only a 10% increase in its fluorescence intensity as compared to the intensity of the same sample after it had been shifted to 37 °C at the end of the experiment. Therefore, A215 was not inserting significantly into the membrane at 4 °C since we have previously shown that the increase in fluorescence intensity of the NBD located at position 215 is unambiguously associated with its membrane insertion.

To determine whether other residues within TMH1, as well as residues in TMH2, also did not appreciably insert into the membrane at 4 °C, we also measured the change in fluorescence intensity of NBD located at positions occupied by residues S194 and N197 of TMH1 (Figure 4B). S194 and 215 are located on opposite strands of TMH1. N197 is located in the same strand as S194, but unlike S194 and A215, N197 faces the aqueous channel. After 90 min at 4 °C, the fluorescence intensity of the NBD located at position S194 only increased to about 20% of the maximum intensity observed after the sample had been shifted to 37 °C at the end of the experiment. The fluorescence intensity

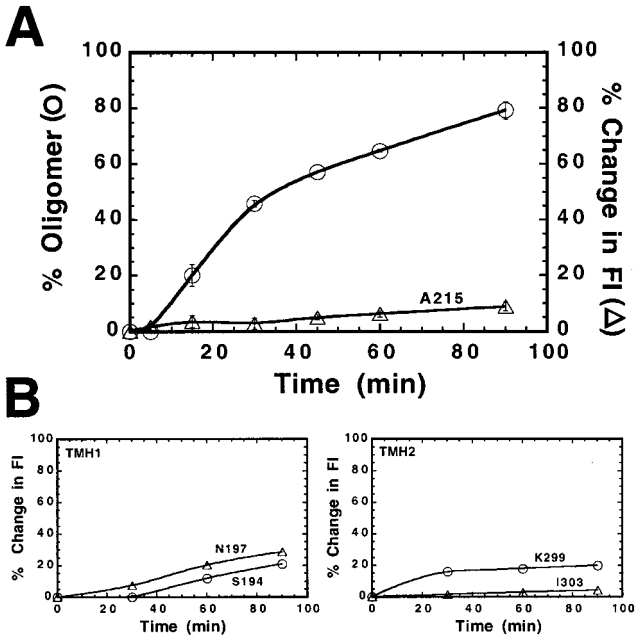

FIGURE 4: Relative rates of oligomer formation and insertion of TMH1 and TMH2 at 4 °C. In panel A, the rate of oligomer formation (circles) at 4 °C was determined by densitometric analysis of the distribution of PFO monomer and its oligomer from SDS−AGE gels similar to those shown in Figure 3A. Simultaneously, the insertion rate of TMH1 (triangles) was determined by examining the increase in the fluorescence intensity of NBD-labeled PFO^{A215C}, shown previously to face the membrane after membrane insertion of PFO (*9*). As described under Materials and Methods, two aliquots were removed from the PFO−liposome sample mixture, which was held at 4 °C, at the times indicated. One of the samples was immediately placed into SDS-sample buffer to stop the process of oligomerization. The other sample was immediately added to 2 mL of HBS buffer in a fluorometer cuvette which had been chilled to 4 °C in the sample chamber of the fluorometer. The fluorescence intensity was measured within 10 s of the addition of the sample to the cuvette. After the last aliquots were removed at the 90 min sampling time, the remaining mixture was heated to 37 °C for 20 min to allow oligomerization and insertion to go to completion. Two final aliquots were then removed and analyzed in the same manner as the previous samples. The fluorescence intensity of the sample incubated at 37 °C was determined at 4 °C to minimize any effects of temperature on the fluorescence intensity of the sample. The values obtained after incubation of the sample at 37 °C were taken as the 100% values for oligomerization and insertion. All values obtained for the aliquots removed during the 4 °C incubation were calculated as a percentage of these final values and are represented as percent oligomer formation and percent change in fluorescence intensity (FI). In panel B, the extent of insertion of other residues within TMH1and TMH2 was also examined in the same fashion as for A215 described above. In the left panel, the change in the fluorescence intensity of NBD located at position 194 of TMH1 was determined at 4 °C. S194 also faces the membrane when PFO inserts into the membrane, but is located in the first β-strand of TMH1 whereas A215 is located in the second β-strand. N197, also located in the first strand of TMH1, faces the channel when TMH1 is inserted into the membrane and so enters into a more polar environment in the oligomer (*9*). In the right panel, the extent of insertion of two residues, K299 and I303, was also determined at 4 °C. Both of these residues have been previously shown to face the membrane in TMH2 and are on opposite strands of the TMH2 hairpin (*10*).

of N197 also changed only about 30%, but in this case the NBD fluorescence intensity decreases because this residue moves from a somewhat hydrophobic location in the monomer to a more hydrophilic position facing the channel. Therefore, this channel-facing residue does not enter the channel. Therefore, significant TMH1 insertion did not occur until the sample was shifted to 37 °C.

The extent of insertion of the second transmembrane β-hairpin of PFO, TMH2, was also examined at 4 °C (Figure 4B). Two residues located in TMH2, K299 and I303, are located on the opposite strands of TMH2. K299 resides near its predicted turn in the β-hairpin and has been shown to face the membrane (*10*). These residues are sensitive indicators of membrane insertion of TMH2 since their fluorescence intensities increase 40−45-fold upon membrane insertion of TMH2. NBD located at position 299 increased to less than 20% of its maximum intensity when TMH2 is fully inserted whereas NBD at position 303 increased to less than 5% of its maximum intensity. These data indicate that TMH2 also does not appear to insert significantly into the membrane at 4 °C.

In all cases, the fluorescence intensity change measured for these residues within TMH1 and TMH2 indicates that neither membrane-spanning β-hairpin appreciably inserts into the membrane. Based on these observations, we suggest that the PFO oligomer assembly can proceed without significant membrane insertion of the TMHs, consistent with the formation of a prepore oligomer.

Pore Formation by PFO in Planar Bilayers. We also examined the formation of ion-conducting channels by PFO in planar bilayers. If a large preinsertion complex was inserting into the membrane, as suggested by the above experiments, then we should observed the rapid opening of large channels in a planar bilayer. When PFO was exposed to the planar bilayer, a population of comparatively homogeneous channels exhibiting large conductance states was observed as a function of time (Figure 5A). Channels with a similar conductance were also observed at a 10-fold lower concentration of PFO (Figure 5A, inset). At the lower concentration of toxin, the time lag between the individual channel openings was significantly longer, yet these channels opened rapidly and exhibited a conductance state similar to the channels formed at higher PFO concentrations. We did not detect small channels, that may have been formed by the insertion of a dimer or small oligomer, that increased gradually in conductance.

Greater than 70% of the recorded PFO channels exhibited a conductance of 4−6 nS (Figure 5B). No conductance values of less than 2.2 nS were detected for PFO, and greater than 98% of the channels exhibited a conductance of $\geq$3.8 nS. Although channels with a conductance greater than 6 nS were clearly present, their abundance was inversely related to the magnitude of the conductance.

The bilayer data also indicate that a size-dependent threshold for the insertion of the oligomer may exist since few channels were detected with a conductance of less than 4 nS. Oligomers that do not reach this threshold size may only insert into the bilayer at a low efficiency as evidenced by the paucity of channels with conductance states of less than 4 nS. When a comparison is made between the distribution of oligomers observed by SDS−AGE (Figure 5B, inset) and the distribution of conductance states (Figure 5B), a remarkably consistent correlation emerges in which the two distribution patterns parallel one another. Few oligomers are detected below the most abundant oligomer band of the stained gel, and as oligomer size increases the abundance of the oligomer decreases as denoted by the

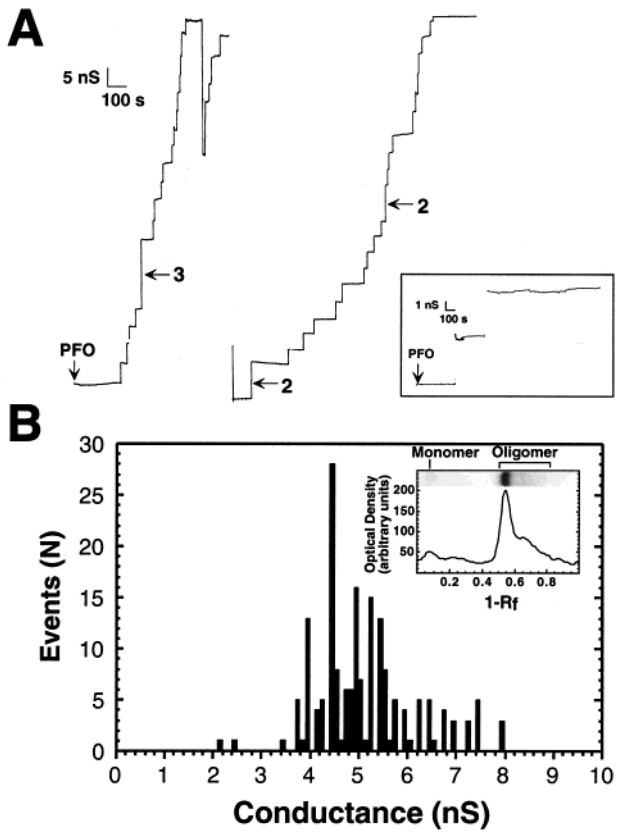

FIGURE 5: Characteristics and distribution of channels formed by PFO^{C459A} in cholesterol−POPC planar bilayers. A typical example of the channels opened by PFO in a cholesterol−POPC bilayer is shown in panel A. PFO concentration was 176 pM in these experiments. We have noted on the recording where 2 or 3 channels opened nearly simultaneously so that these were not mistaken as a single large-conductance channel. In all cases, the experiments were carried out in 0.2 M NaCl with a holding potential of +10 mV. The recording shown in the inset to panel A is a separate experiment in which the concentration of PFO was decreased 10-fold to 17.6 pM in order to generate just a few channels. Two channels are shown, and each exhibited a long stable conductance of over 6 and 21 min prior to the opening of another channel. Conductance and time scales are shown on each recording. Shown in panel B is a histogram of the distribution of conductance states for PFO channels from 7 separate planar membrane experiments (a total of 180 channels were measured). From these experiments, 73% of the channels formed in the bilayer were determined to have conductance states between 4 and 6 nS. Only two channels were detected (1% of the total measured) with conductance states less than 3.8 nS. Shown in the inset in panel B is a densitometry trace of the PFO oligomer distribution from the SDS−agarose gel shown in Figure 1, lane 6. As can be seen, the distribution of observed conductance states for PFO closely follows the distribution pattern of the oligomeric complexes detected by SDS−AGE.

gradually decreasing intensity of the stain. Similarly, few channels are observed with conductance states of less than 4.0 nS, and the probability of channels with conductances greater than 6 nS decreases with increasing conductance.

DISCUSSION

The CDCs represent a novel family of pore-forming toxins that create oligomeric complexes and pores that are significantly larger than other characterized pore-forming toxins and permit the passage of molecules as large as hemoglobin (*28*) and IgG (*29*) [reviewed in (*30*)]. Because of the large size of the membrane oligomer generated by the CDCs, the mechanism of membrane assembly and insertion of these large homooligomeric complexes has been a subject of debate (*8, 18*). Rossjohn et al. (*8*) originally proposed a prepore model for the assembly of PFO into its oligomer (Figure 6A). This mode of membrane insertion has been shown to operate for a variety of pore-forming toxins (*12*−*14, 27*). The basic tenet of the prepore mechanism is that the oligomer forms prior to significant insertion of the β-barrel. However, Palmer et al. (*18*) proposed an alternative assembly mechanism for the CDCs, primarily due to conceptual problems envisioned for the assembly and insertion of the large oligomeric complex of the CDCs. They proposed that the membrane insertion of a CDC dimer initiated oligomer and pore formation (Figure 6B). The dimer, or small oligomer, thus forms a small pore that is then gradually enlarged by the addition of CDC monomers to the primary insertion complex. Therefore, in contrast to the prepore model, oligomer growth is inextricably linked to the insertion of the transmembrane β-hairpins into the bilayer.

Initially we examined the size distribution of PFO oligomers on liposomal membranes. Using SDS−AGE, it was possible to resolve and quantify the distribution of PFO oligomers at a level of detail that was not previously possible using methods such as EM or sucrose density centrifugation. The results of these analyses showed that PFO forms a large, relatively uniform-sized oligomer. Although oligomers larger than the predominant oligomer can form, the frequency with which they occur is significantly less than that observed for the predominant PFO oligomer. Interestingly, oligomers smaller than the predominant oligomer were virtually undetectable, except by sensitive antibody-based detection methods. As evidenced by the predominant single oligomer band observed using SDS−AGE, there is a strong tendency for PFO monomers to form an oligomer of a specific size. As described above, the small oligomers of toxins such as α-toxin, aerolysin, α-hemolysin, and anthrax PA form discrete-sized prepore oligomers of 6−7 monomers. Although the CDCs form much larger oligomers and membrane pores, our results indicate that a minimum size of oligomer may be required for membrane insertion of the β-barrel. The continuous growth model of Palmer et al. (*18*) predicts a prevalence of dimers or small oligomers during the early stages of oligomer assembly; however, this is not what we observed. Although these data do not rule out either model of assembly, they are most consistent with the formation of a prepore complex.

We also examined the relationship between PFO oligomerization and the insertion of the membrane-spanning β-hairpins of PFO. Low temperature was used to resolve the oligomerization and insertion processes. The oligomerization of PFO was slowed by lowering the temperature to 4 °C, but the extent of oligomerization was still significant. After 90 min at 4 °C, nearly 80% of the PFO monomer had been converted into the same large oligomer observed at 37 °C. However, during the same time period, we could only detect a 5−28% change in the fluorescence of four membrane-facing and one channel-facing residue that are located within the membrane-spanning β-hairpins, indicating that only a fraction may have inserted into the membrane. The oligomeric complex formed at 4 °C was essentially identical, in its size and its resistance to dissociation by SDS, to the oligomer formed at 37 °C. Apparently the formation

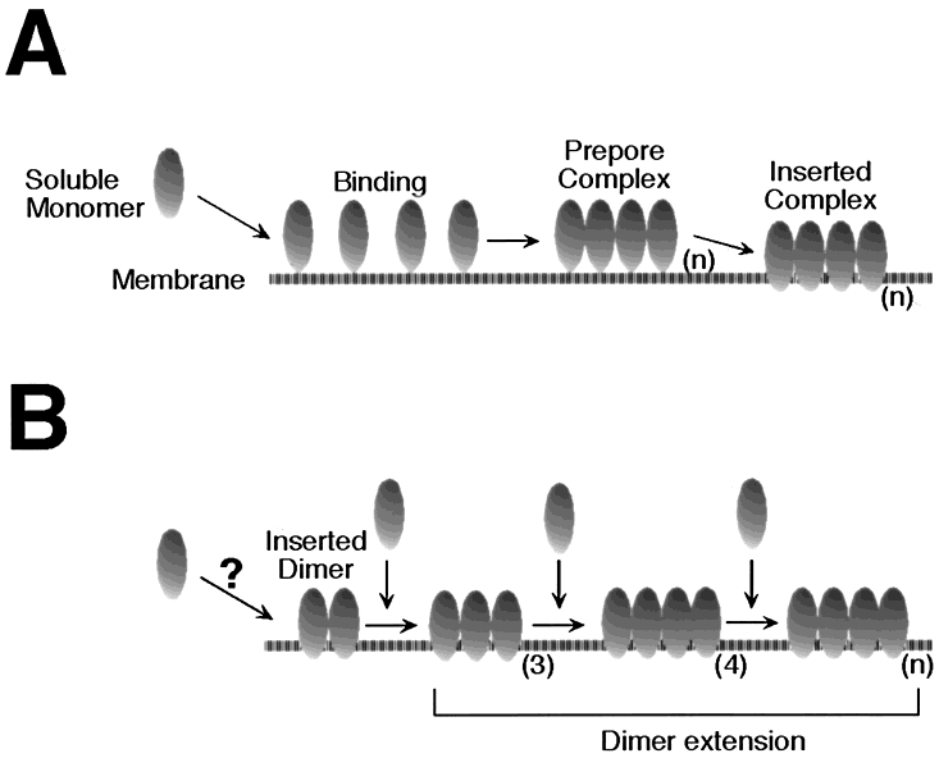

FIGURE 6: Models of membrane insertion for the CDCs. Shown are the prepore model of Rossjohn et al. (*8*) (panel A) and the continuous growth model of Palmer et al. (*18*) (panel B) for the assembly and insertion of a CDC. (n) represents the number of monomers comprising the oligomer.

of the β-sheet was not involved in defining the size, or stability to SDS, of the oligomeric structure. Thus, PFO can indeed assemble into a large oligomeric complex in the absence of significant insertion of its membrane-spanning β-hairpins. These results are consistent with the key feature of the prepore model, that oligomerization can proceed in the absence of significant insertion of the transmembrane β-sheet. However, they are not consistent with the continuous growth model where oligomer assembly proceeds only upon the insertion of the transmembrane β-hairpins of each monomer as it is added to the oligomer.

The results of the planar membrane analysis show that PFO forms large, relatively homogeneous channels in planar membranes comprised of cholesterol and POPC. The PFO-dependent channels opened rapidly and exhibited large conductance states, consistent with the insertion of a single, large pore-forming complex into the bilayer. For comparison, the single-channel conductances of the channels formed by aerolysin (*31*, *32*), *Clostridium septicum* α-toxin (*22*), and *Staphylococcus aureus* α-hemolysin (*33*) were more than 10 times lower (0.070−0.200 nS) than those of the PFO channels. In addition, when only a few channels were formed at low concentrations of PFO, these channels exhibited the same conductance as those formed at 10-fold higher concentrations. We did not observe small conductance patterns during these analyses, a feature that is predicted by the continuous growth model. The paucity of small channels was particularly evident when only a few channels were formed. Long periods of stable conductance were observed prior to the rapid appearance of large channels as discrete events. These channels exhibited the same conductance as those formed at higher toxin levels. The formation of these channels by means other than the insertion of a prepore complex is difficult to envision.

When the findings of the current study are taken in toto, they strongly support the formation of a large oligomeric prepore as a prerequisite for insertion of the pore-forming, membrane-spanning β-sheet of PFO. We propose that PFO, and probably all CDCs, use a membrane insertion mechanism based on the formation of a prepore complex. These findings also suggest that the formation of a prepore oligomeric complex may be a fundamental biological mechanism that can facilitate the insertion of a wide range of sizes of transmembrane β-sheets.

ACKNOWLEDGMENT

We thank Dr. Alejandro Heuck for his advice and assistance in these studies.

REFERENCES

1. Tweten, R. K. (1995) in *Virulence Mechanisms of Bacterial Pathogens* (Roth, J. A., Bolin, C. A., Brogden, K. A., Minion, C., and Wannemuehler, M. J., Eds.) pp 207−230, American Society for Microbiology, Washington DC.
2. Rossjohn, J., Tweten, R. K., Rood, J. I., and Parker, M. W. (1999) in *Bacterial Toxins: A Comprehensive Sourcebook* (Alouf, J., and Freer, J., Eds.) pp 406−420, Academic Press, London.
3. Alouf, J. E., and Geoffrey, C. (1984) in *Bacterial Protein Toxins* (Alouf, J. E., Fehrenbach, F. J., Freer, J. H., and Jeljaszewicz, J., Eds.) pp 165−171, Academic Press, London.
4. Duncan, J. L., and Schlegel, R. (1975) *J. Cell Biol. 67*, 160−174.
5. Morgan, P. J., Hyman, S. C., Byron, O., Andrew, P. W., Mitchell, T. J., and Rowe, A. J. (1994) *J. Biol. Chem. 269*, 25315−25320.

6. Sekiya, K., Satoh, R., Danbara, H., and Futaesaku, Y. (1993) *J. Bacteriol. 175*, 5953−5961.
7. Bhakdi, S., Tranum, J. J., and Sziegoleit, A. (1985) *Infect. Immun. 47*, 52−60.
8. Rossjohn, J., Feil, S. C., McKinstry, W. J., Tweten, R. K., and Parker, M. W. (1997) *Cell 89*, 685−692.
9. Shepard, L. A., Heuck, A. P., Hamman, B. D., Rossjohn, J., Parker, M. W., Ryan, K. R., Johnson, A. E., and Tweten, R. K. (1998) *Biochemistry 37*, 14563−14574.
10. Shatursky, O., Heuck, A. P., Shepard, L. A., Rossjohn, J., Parker, M. W., Johnson, A. E., and Tweten, R. K. (1999) *Cell 99*, 293−299.
11. Garland, W. J., and Buckley, J. T. (1988) *Infect. Immun. 56*, 1249−1253.
12. Valeva, A., Pongs, J., Bhakdi, S., and Palmer, M. (1997) *Biochim. Biophys. Acta 1325*, 281−286.
13. Sellman, B. R., Kagan, B. L., and Tweten, R. K. (1997) *Mol. Microbiol. 23*, 551−558.
14. Miller, C. J., Elliot, J. L., and Collier, R. L. (1999) *Biochemistry 38*, 10432−10441.
15. Petosa, C., Collier, R. J., Klimpel, K. R., Leppla, S. H., and Liddington, R. C. (1997) *Nature 385*, 833−838.
16. Song, L. Z., Hobaugh, M. R., Shustak, C., Cheley, S., Bayley, H., and Gouaux, J. E. (1996) *Science 274*, 1859−1866.
17. Olofsson, A., Hebert, H., and Thelestam, M. (1993) *FEBS Lett. 319*, 125−127.
18. Palmer, M., Harris, R., Freytag, C., Kehoe, M., Tranum-Jensen, J., and Bhakdi, S. (1998) *EMBO J. 17*, 1598−1605.
19. Harris, R. W., Sims, P. J., and Tweten, R. K. (1991) *J. Biol. Chem. 266*, 6936−6941.
20. MacDonald, R. C., MacDonald, R. I., Menco, B. P. M., Takeshita, K., Subbarao, N. K., and Hu, L.-R. (1991) *Biochim. Biophys. Acta 1061*, 297−303.
21. Laemmli, U. K. (1970) *Nature (London) 227*, 680−685.
22. Ballard, J., Sokolov, Y., Yuan, W.-L., Kagan, B. L., and Tweten, R. K. (1993) *Mol. Microbiol. 10*, 627−634.
23. Hoyer, L. W., Rizza, C. R., Tuddenham, E. G., Carta, C. A., Armitage, H., and Rotblat, F. (1983) *Br. J. Haematol. 55*, 493−507.
24. Kornberg, A., Francis, C. W., and Marder, V. J. (1992) *Blood 80*, 709−717.
25. Hugo, F., Reichwein, J., Arvand, M., Krämer, S., and Bhakdi, S. (1986) *Infect. Immun. 54*, 641−645.
26. Thelestam, M., Olofsson, A., Blomqvist, L., and Hebert, H. (1991) *Biochim. Biophys. Acta 1062*, 245−254.
27. Van der Goot, F. G., Pattus, F., Wong, K. R., and Buckley, J. T. (1993) *Biochemistry 21*, 2636−2642.
28. Duncan, J. L. (1974) *Infect. Immun. 9*, 1022−1027.
29. Hamman, B. D., Chen, J. C., Johnson, E. E., and Johnson, A. E. (1997) *Cell 89*, 535−544.
30. Bhakdi, S., Weller, U., Walev, I., Martin, E., Jonas, D., and Palmer, M. (1993) *Med. Microbiol. Immunol. (Berlin) 182*, 167−175.
31. Chakraborty, T., Schmid, A., Notermans, S., and Benz, R. (1990) *Infect. Immun. 58*, 2127−2132.
32. Wilmsen, H. U., Pattus, F., and Buckley, J. T. (1990) *J. Membr. Biol. 115*, 71−81.
33. Menestrina, G. (1986) *J. Membr. Biol. 90*, 177−190.

BI000436R